A Low RCS Wideband Antenna Based on Share-structure of FSA and ME-dipole

Youquan Wen, Sai-Wai Wong, Huawei Lin, Chunlin Ji, Ruopeng Liu, and Yejun He

***Abstract*—A wideband integrated antenna is proposed with realization of radiation and dual polarized absorption in same frequency band. The novelty of the proposed integrated structure lies in the share-aperture of frequency-selective absorber and magnetoelectric dipole, which remain mutually independent and orthogonal operating characteristics. In the share-structure, each array element can be selectively connected to an excitation port or a resistor loading (50 Ω) to re-use the antenna port impedance for receiving and absorbing co-polarized waves. While the cross-polarized waves are reflected by antenna ground and absorbed by mounted resistors on the symmetric patches at the top layer of the antenna array. Consequently, the proposed antenna exhibits both wideband radiation and dual polarized absorption simultaneously with low profile ($0.22\lambda_0$). Finally, a prototype 2×2 antenna array is fabricated and measured, demonstrating an impedance bandwidth of 92.7% for |S11| < −10 dB from 2.2 to 6 GHz. Moreover, the proposed antenna has 10 dB RCS reduction bandwidth of 100% (2-6 GHz) for x- and y-polarized normally incident waves.**

***Index Terms*—frequency-selective absorber (FSA), wideband antenna, radar cross section (RCS).**

I. Introduction

Recently, stealth performance of communication equipment is crucial in military applications related to detection and communication [1]. Low radar cross section (RCS) antennas have gained significant traction in integrated sensing and communication by effectively reducing the target signature of military communication equipment under radar detection [2]. A common approach for RCS reduction of antenna involves the use of metasurface to scatter the incident electromagnetic (EM) wave to lower the EM radiation energy in particular directions or absorb EM energy[3], [4].

For the first category, a variety of checkerboard arrays such as artificial magnetic conductors (AMC) [5], polarization converter [6], [7] and coding metasurfaces [8] find extensive applications in RCS reduction. For another, frequency-selective absorbers (FSAs) have been proposed in the literature, also offering the advantage of reducing the RCS [9]-[10]. FSAs are placed above the antenna, which allow the passage of in-band waves and absorb out-of-band waves. However, achieving low in-band RCS of antenna remains a challenge, as it involves a significant trade-off between radiation and absorption characteristics. In [11]-[15], these common methods such as using polarization rotation reflective surfaces to isolate col-polarized and cross-polarized waves, or using diodes to switch the radiation and absorption states. However, aforementioned structures are using separated circuit and separated layer which leads to a higher profile. And those FSAs usually exhibit a narrow frequency response and filtering characteristics, which impose constraints on the antenna bandwidth or radiation efficiency. Therefore, it is of great significance to design a low-profile wideband antenna that possesses the advantages of both wideband operation and low RCS using FSA technique.

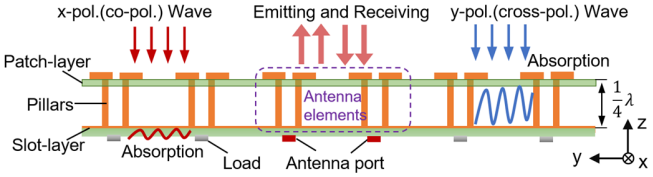

Fig. 1. Schematic model of integrated array antenna (Section view of x = 0)

In recent years, it has been a tendency to focus excessively on improving FSA designs to achieve in-band low RCS for antennas, which has led to a fixed mindset. In contrast, the inherent characteristics and design aspects of the antenna itself are usually overlooked or underestimated. Magnetoelectric dipole (ME-dipole) consists of the horizontal patch (operate as electric dipole) and vertical quarter-wave shorted metallized vias (operate as magnetic dipole) [16]. For ME-dipoles, the ideal height is typically chosen to be a quarter electrical length (λ_l /4) for optimal matching performance and good radiation pattern [17]. As for the design of FSA, the thickness is also commonly corresponding to a quarter wavelength (λ_f /4) of the resonant frequency, enabling the FSA to achieve a maximum absorption of specific frequencies of EM waves. Therefore, the integrated structure of FSA and ME-dipole can achieve wideband radiation for communication and wideband absorption for low RCS performance simultaneously.

In this letter, a wideband integrated antenna is proposed with dual-function of radiation and absorption in same frequency band. The shared-structure of the FSA and ME-dipole is adopted to achieve the share-aperture, resulting in a compact and lower-profile design when compared with reported works that involve stacking separate circuits and layers. Moreover, both FSA and antenna have wideband performance with both functions more than fractional bandwidth (FBW) of 92.7% and overlapping the same wideband frequency in this proposed work.

This work is supported by the National Natural Science Foundation of China under grant 62171289. (Corresponding author Sai-Wai Wong, e-mail: wongsaiwai@ieee.org).

Y. Wen, S.W. Wong, and Y. He are with State Key Laboratory of Radio Frequency Heterogeneous Integration, Guangdong Engineering Research Center of Base Station Antennas, Shenzhen Key Laboratory of Antennas and Propagation, College of Electronics and Information Engineering, Shenzhen University, Shenzhen 518060, China.

H. Lin is with the Faculty of Science and Technology, University of Macau, Taipa, Macau.

C. Ji and R. Liu are with Kuang-Chi Institute of Advanced Technology, Shenzhen 518000, China.

This article has been accepted for publication in IEEE Antennas and Wireless Propagation Letters. This is the author's version which has not been fully edited and content may change prior to final publication. Citation information: DOI 10.1109/LAWP.2024.3383853

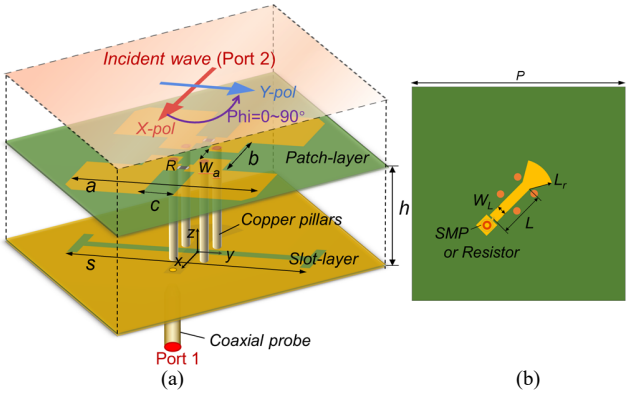

Fig. 2. Unit cell of the proposed integrated antenna. (a) 3-D view of the proposed integrated antenna and FSA, (b) bottom view of the slot-layer. (Structure parameters: P = 45.2, a= 32, b= 11, c = 7, w_a = 2.5, s = 32, W_L = 2.4, L = 13.3, L_r = 6.5, h = 16, all in mm; R = 225 Ω.

II. Geometry And Analysis Of Antenna Element

Fig. 1 illustrates the schematic model of integrated array antenna. The proposed antenna acts as a share-structure base on ME-dipole and FSA, which consist of patch-layer loaded with resistors, vertical metallized pillars and slot-layer. For radiation, the proposed arrays are excited by aperture-coupled feeding on center elements of slot-layer. Each array element can be selectively connected to an excitation port or a resistor loading (50 Ω) to re-use the antenna port impedance for receiving. For incident wave, the integrated structure can be regard as a frequency-selective absorber. The co-polarized wave can be received through the slot, and be absorbed by resistors of 50 Ω on rest elements of slot-layer. While the cross-polarized waves are reflected by antenna ground and absorbed by mounted resistors on the symmetric patches at the top layer of the antenna array. Thus, both the co-polarized and cross-polarized waves are absorbed by the integrated structure. Consequently, the proposed antenna exhibits both wideband radiation and low in-band radar cross-section.

Fig. 2 illustrate the geometry of the unit cell of integrated antenna. As is shown in Fig. 2 (a), the integrated antenna consists of the patch-layer, vertical copper pillars, and the slot-layer. The patch-layer comprises four symmetrical patches are etched on a F4BM substrate with permittivity of 2.65 and thickness of 0.3 mm, which act as E-dipoles. And two pairs of symmetrical patches are designed as a Minkowski island for size reduction [18]. Two resistors are connected the two pairs of patches, which parallel to x-axis. The length of each patch is about a quarter wavelength (λ_f /4) with respected to lower resonant frequency of the antenna, where λ_f is the corresponding wavelength. The vertical copper pillars are mounted between the patch-layer and the feed-layer through metal vias, which work as M-dipoles. The height of vertical copper pillars is denoted as h. The slot-layer incorporates features such as an I-shaped slot and a fan-shaped microstrip line, aimed at achieving miniaturization and broadband matching. The slot is positioned at the center of the four vertical copper pillars and parallel to the y-axis. As shown in Fig. 2(b), the bottom surface of the slot-layer etches a fan-shaped microstrip line with the other side fed by a 50 Ω coaxial probe, and the thickness of slot-layer is 1 mm.

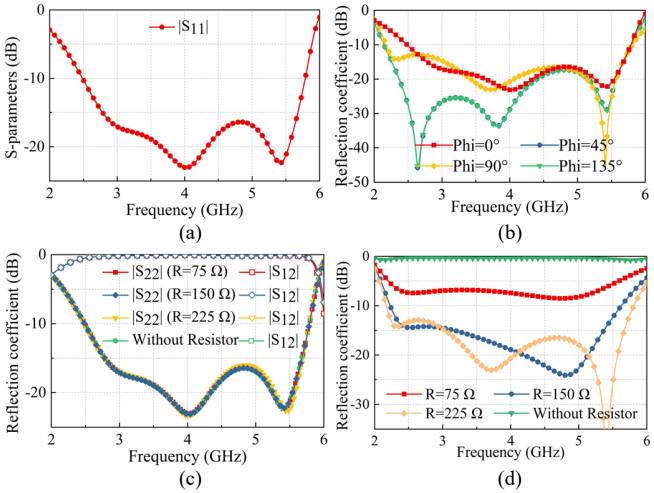

Fig. 3. Simulated results of unit cell of the proposed integrated antenna. (a) $|S_{11}|$, (b) reflection coefficients for different Phi incident waves, (c) reflection coefficients for x-polarized wave with different resistances, (d) reflection coefficients for y-polarized wave with different resistances.

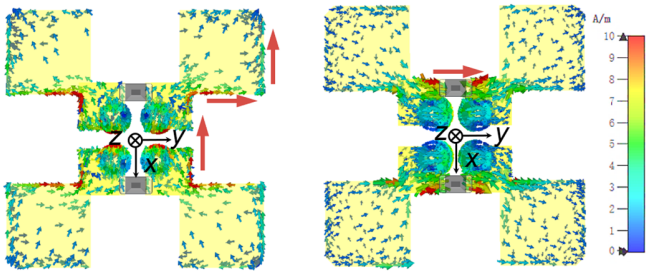

Fig. 4. The current distribution of the proposed integrated antenna at 4 GHz for different polarization. (a) x-polarization, (b) y-polarization.

Fig. 3 shows simulated results of the proposed integrated antenna at the boundary conditions of the unit cell. When Port 1 acts as excitation, it can be seen in Fig. 3 (a) that the antenna achieves an impedance matching bandwidth of 2.5-5.8 GHz (FBW = 79.5%) and transmit to free space. Fig. 3 (b) shows the reflection coefficient, when Port 2 acts as different polarized incident wave from free space. In this condition, the Port 1 acts as a resistor loading of 50 Ω, thus the reflection coefficient ($|S_{22}|$) can represent absorption. When Phi = 0 (x-polarized wave), it can be seen that the reflection coefficient is the same result as in Fig. 3 (a). According to the antenna reciprocity, it also indicates that the x-polarized incident wave (co-polarized wave) has entered the slot-layer and been absorbed by Port 1 [19]. When Phi = 90 (y-polarized wave, or cross-polarized incident wave), the reflection coefficient is less than -10 dB over the frequency range of 2.2-5.8 GHz (FBW = 90%). Moreover, the reflection coefficients for different Phi incident waves are stable. It can be indicated that the proposed antenna has wideband absorption for any polarized incident wave. Fig. 3(c) and Fig. 3(d) respectively show the reflection coefficients for x-polarization and y-polarization with different resistances of R. It can be seen that the result for x-polarization is not affected by the value of surface resistors, incident wave smoothly is absorbed by Port 1. For y-polarization, when no resistor is added, incident wave is full reflected back. It illustrates that the y-polarized waves can be reflected by the slot-layer (acts as ground) and then be absorbed by patch-layer loaded with

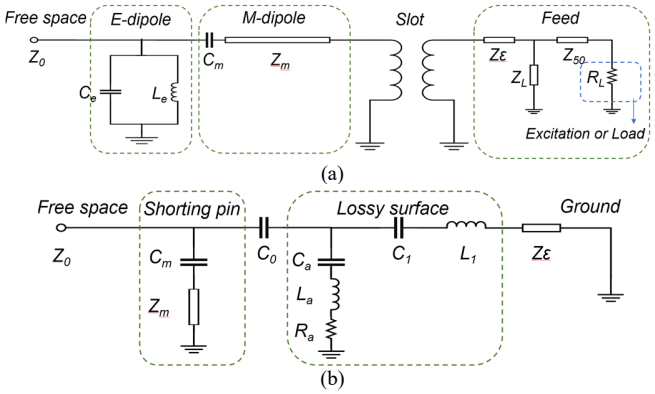

Fig. 5. Equivalent circuit model for (a) x-polarization, (b) y-polarization.

resistors. When R = 225 Ω, the results reach maximum absorption bandwidth.

The surface current at 4 GHz for y-polarized wave is presented in Fig. 4 (b). The surface current is concentrated at the edges of the patches (parallel to the y-axis), while the current at the outer edges (parallel to the x-axis) is very weak. It can be observed that the location of current concentration is precisely different from the distribution in Fig.4 (a). Therefore, it can be inferred that the radiation characteristics of the antenna and the absorption properties of the FSA remain mutually independent and orthogonal. In consequence, it verifies the feasibility of the share-aperture based on ME-dipole and the FSA, preliminarily.

The equivalent circuit model is regarded as an efficient way to analyze the reflection behavior for the incident waves with two different polarizations. For the x-polarization, Fig. 5 (a) presents the equivalent circuit model of the structure, which work as the ME-dipole. As the model, the impedance of the free space and the dielectric substrate can be equivalent to Z_0 and Z_ε. The patch-layer can be seen as an LC parallel circuit, where the inductor L_e denotes the patches, and the capacitor C_e denotes the gap between the adjacent patches. In this model, the resonant frequency f is determined by the following formula [13]:

$$f = \frac{1}{2\pi\sqrt{L_e C_e}} \tag{1}$$

and the characteristic impedance of Z_e can be determined by the formula [23]

$$Z_e = \sqrt{\frac{L_e}{C_e}} \tag{2}$$

By adjusting the values of capacitance and inductance, specific resonant frequencies can be achieved, enabling the antenna to have higher radiation efficiency and optimal impedance matching at operating frequency. The capacitor C_m denotes the discontinuous coupling structure between the patches and the pillar. The transmission line with the impedance of Z_m denotes the vertical pillars between the patch-layer and the feed-layer, which is determined by the formula [16]:

$$Z_m = \frac{1}{2} Z_d = \frac{60}{\sqrt{\varepsilon_r}} arcosh\left(\frac{D_r}{2r_0}\right) \tag{3}$$

where ε_r is the relative permittivity, D_r is the center spacing of two adjacent copper pillars, and r_0 is the diameter of the copper pillar. The slot on the frontside of the feed-layer is equivalent

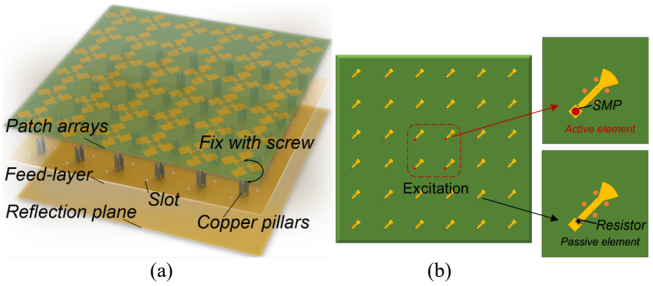

Fig. 6. The geometry of integrated antenna arrays.
(a) Schematic view of assembly structure, (b) bottom view of feed-layer.

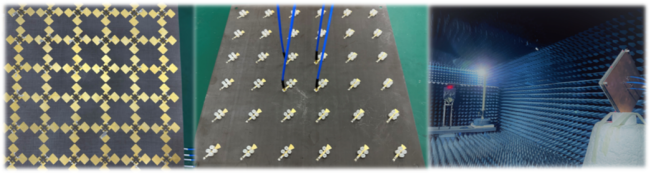

Fig. 7. Prototype of integrated antenna arrays. (a) top view of patch arrays, (b) the feed-layer of 2×2 excited arrays, (c) photograph of the measurement setup.

to a transformer. Lastly, the feeding network on the backside of the feed-layer can be denoted as a microstrip transmission line Z_L connected in parallel with a matching load R_L. Fig. 5 (b) presents the equivalent circuit model for the y-polarization. For the y-polarized waves, it can be regarded as the FSA mentioned previously [20]. The patch-layer can be equivalent to a lossy surface instead of E-dipole. In the lossy surface, the inside edges of the patches connected resistors form an RLC series circuit, with the other end grounded. And the outer boundary of the patches is equivalent to a capacitor C_1 in series with an inductor L_1. Besides, the capacitor C_m and the transmission line Z_m can be considered as the M-dipole, which is in series with ground. Based on these correlations between circuit and size parameters, it has obtained optimized parameters for the proposed shared-structure as shown in Fig. 2.

III. Antenna Array and Experimental Results

A. The Integrated Structure of Antenna Arrays

Fig. 6(a) presents the geometry of integrated structure of antenna arrays. The structure is composed of 6 × 6 unit cells with checkerboard arrays. The overall size of the structure is $3.73\lambda_0 \times 3.73\lambda_0 \times 0.36\lambda_0$ (λ_0 is the wavelength at the center frequency of 4 GHz in free space). The patch arrays and copper pillars are fixed with screws, which work as ME-dipole arrays. As shown in Fig. 6(b), 2×2 antenna elements in the center are excited by the aperture-coupled feeding with 50 Ω port impedance. And the rest of unexcited feedings are terminated with resistors loading of 50 Ω. The prototype of the integrated structure is fabricated and presented in Fig. 7. Furthermore, this integrated structure can excite an arbitrary number of antenna elements. Besides, the addition of the reflection copper plate below the feed-layer serves to reduce backward radiation and diffraction which didn't affect the absorber performance. To verify this feasibility, the feed-layer with 2×2 excited antenna elements are designed to be driven by four coaxial ports in Fig. 7(b). It is noteworthy that, 2×2 antenna array is only an example. The number of antenna array elements can be arbitrary chosen, e.g., 4×4 antenna array elements as well. And it can be adopted

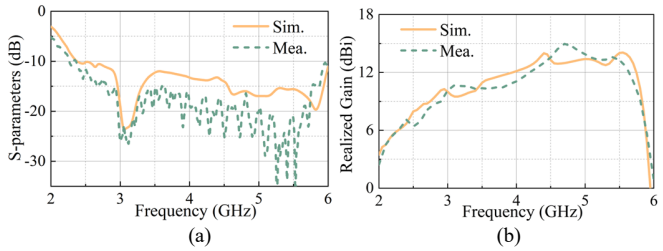

Fig. 8. (a) Simulated and measured S-parameters of 2×2 excited arrays, (b) Simulated and measured gains of 2×2 excited arrays.

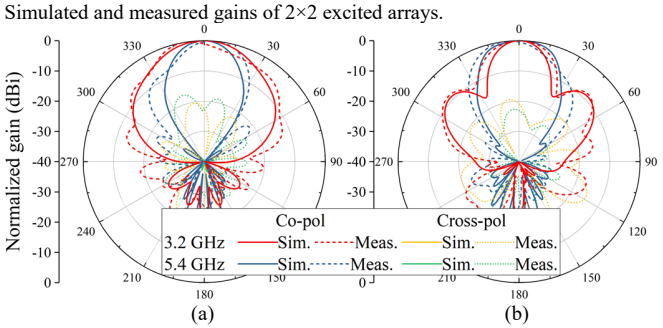

Fig. 9. Simulated and measured radiation patterns of 2×2 excited arrays at (a) xoz plane, and (b) yoz plane.

to increase the gain by connecting antenna elements to feeding port through power divider network.

B. Radiation Performance

For the 2×2 excited arrays, Fig. 8 (a) illustrates the simulated and measured S-parameters. The simulated impedance bandwidth is 89.2%, with $|S_{11}| < -10$ dB from 2.3 to 6 GHz. The measured impedance bandwidth is about 92.7%, with $|S_{11}| < -10$ dB from 2.2 to 6 GHz. A good agreement has been obtained between the simulated and the measured results. Fig. 8(b) presents the realized gain of the 22 excited arrays, which shows the consistent trend of measured results and simulated ones. Some deviations may arise from dielectric losses, installation tolerance, as well as environment uncertainties. Fig. 9 gives the radiation patterns at 3.2 and 5.4 GHz, respectively. The radiation patterns of the antenna array remain relatively stable across two frequency bands. The cross-polarization levels of measurements are below -20 dB in both the xoz-plane and yoz-plane. By comparing measured and simulated results, it can be observed a good agreement between them.

C. Scattering Performance

To verify the absorption of the proposed antenna, the reflection coefficients under different oblique incidences are measured by the arch-method [24]. In Fig. 10, it can be noticed that the prototype shows stable reflection coefficient when the oblique incidence is less than 30° under both x- and y-polarization (TM and TE modes) [21], [25]. Furthermore, in order to show the effect of the proposed antenna for RCS reduction, both the monostatic RCS of the proposed antenna are investigated and compared with the reference antenna. Fig. 7 (c) illustrates the measurement setup in an anechoic chamber. The fabricated antenna prototype is vertically positioned on a foam platform and terminated with a matched load. Differing from the proposed antenna, the reference antenna lacks the installation of ME-dipole arrays and resistors on the feed-layer. Fig. 11 respectively depicts the monostatic RCS results. For the x-polarization, the proposed antenna achieves RCS reduction of

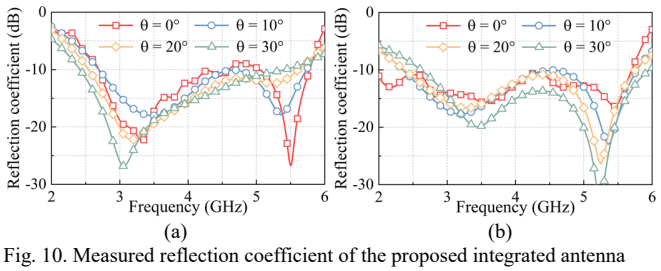

Fig. 10. Measured reflection coefficient of the proposed integrated antenna under different oblique incidences. (a) x- and (b) y-polarization.

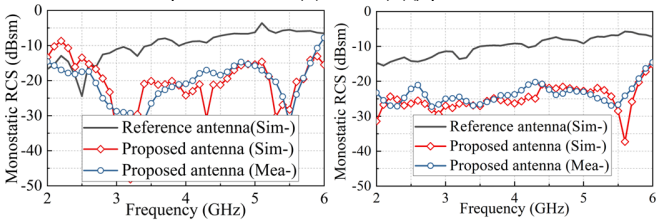

Fig. 11. Simulated and measured monostatic RCS the proposed integrated antenna. (a) x- and (b) y-polarization.

TABLE I
COMPARISONS OF PARAMETERS AMONG LOW-RCS ANTENNAS

Ref.	Structure	Impedance, FBW	Size($\lambda_0\times\lambda_0\times\lambda_0$)	RCS reduction, FBW
[11]	HMS+antenna	9.5-10.2 GHz, 7.1%	2.2×2.2×0.8	6-18 GHz (>5 dB), 100%
[14]	Reconfigurable FSA+antenna	8.15-8.5 GHz, 3.6%	1.88×2.08×0.2	4.02-13.82 GHz (>10 dB), 101%
[15]	FSA+CP antenna	4.5-5.7 GHz, 23.5%	1.89×1.89×0.23	2.5-5.7 GHz (>10 dB), 78%
[22]	ATFSS+F-P cavity antenna	7.3-7.7 GHz, 5.3%	2×1.75×0.8	4-7.2 GHz (>5 dB), 57.1%
This work	FSA&ME-dipole	**2.2-6 GHz, 92.7%**	3.73×3.73×0.22	2-6 GHz (>10dB), 100%

10 dB from 2.8 to 6 GHz (FBW=72.7%). For the y-polarization, it achieves a low RCS band from 2 to 6 GHz (FBW=100%). It indicates that a wideband RCS reduction is obtained for both of x-polarized and y-polarized incident waves. Finally, to better understand the attractive advantages of the proposed integrated device, a comparative study with other reported low-RCS antennas is tabulated in Table I. The comparison with other reported works has validated the effectiveness of the proposed structure in design of low-RCS antennas. The proposed antenna has the widest impedance FBW of 92.7% and comparable low profile as well as wide RCS reduction FBW of 100%.

IV. CONCLUSION

In this letter, the low RCS wideband antenna based on the share-structure of FSA and ME-dipole has been proposed and fabricated. The integrated structure appears to be well-designed for both antenna radiation and FSA absorption, simultaneously. The performances of antenna are measured and analyzed. The results demonstrate that the proposed antenna has broadband impedance bandwidth and RCS reduction when it compares with reported works. Overall, the proposed work can address the challenges of wireless communication and in-band RCS reduction effectively, and the design of share-structure is verified to be a promising approach in low-profile and wideband integrated devices.

REFERENCES

[1] E. F. Knott, J. F. Shaeffer, and M. T. Tuley, *Radar Cross Section*. Stevenage, U.K.: SciTech, 2004.

[2] L. Gan, W. Jiang, Q. Chen, X. Li, Z. Zhou and S. Gong, "Method to Estimate Antenna Mode Radar Cross Section of Large-Scale Array Antennas," *IEEE Trans. Antennas Propag.*, vol. 69, no. 10, pp. 7029-7034, Oct. 2021.

[3] Y. Azizi, et al., "Wideband RCS reduction by single-layer phase gradient modulated surface," *Sensors*, vol. 22, no. 19, pp. 7108, 2022.

[4] X. Xu, S. Ma, X. Ling, X. K. Zhang, S. Tang, T. Cai, et al., "Deterministic approach to achieve broadband polarization-independent diffusive scatterings based on metasurfaces," IEEE Access, vol. 5, no. 5, pp. 1691-1702, 2017.

[5] Y. F. Cheng, L. Yang, X. Zhong, C. Liao and X. Ding, "Analysis and Design of Wideband Low-RCS Fabry–Perot Antennas With Reduced Profile," *IEEE Trans. Antennas Propag.*, vol. 70, no. 9, pp. 7934-7943, Sept. 2022, doi: 10.1109/TAP.2022.3177488.

[6] M. K. T. Al-Nuaimi, et al., "Design of Polarization-Insensitive and Angularly Stable Metasurfaces with Symmetric Cubic Phase Distribution for Broadband RCS Reduction," *IEEE Trans. Antennas Propag.*, vol. 71, no. 11, pp. 9783-9791, 2023.

[7] M. K. T. Al-Nuaimi, Yejun He, and Wei Hong, "Scattered EM-wave shaping using combination of cross-polarization conversion and reflection phase cancellation," IEEE Antennas Wireless Propag. Lett., vol. 18, no. 2, pp. 318-322, Feb. 2018.

[8] M. K. T. Al-Nuaimi, et al., "Coding Engineered Reflector for Wide-band RCS Reduction under Wide Angle of Incidence," *IEEE Trans. Antennas Propag.*, vol. 70, no. 10, pp. 9947-9952, Oct. 2022.

[9] He Y, Jiang J, Chen M, et al. "Design of an adjustable polarization-independent and wideband electromagnetic absorber, " *J. Appl. Phys.*, vol. 119, no. 10, pp. 105103, March 2016.

[10] Y. Pang et al., "Wideband RCS Reduction Metasurface With a Transmission Window," *IEEE Trans. Antennas Propag.*, vol. 68, no. 10, pp. 7079-7087, Oct. 2020.

[11] Y. Liu, Y. Jia, W. Zhang and F. Li, "Wideband RCS Reduction of a Slot Array Antenna Using a Hybrid Metasurface," *IEEE Trans. Antennas Propag.*, vol. 68, no. 5, pp. 3644-3652, May 2020.

[12] M. Li, Z. Yi, Y. Luo, B. Muneer and Q. Zhu, "A Novel Integrated Switchable Absorber and Radiator," *IEEE Trans. Antennas Propag.*, vol. 64, no. 3, pp. 944-952, March 2016.

[13] J. Sun, Q. Cao, Y. Li and H. Li, "Functional Reconfigurable Integrated Structure of Circularly Polarized Antenna and FSS Absorber," *IEEE Trans. Antennas Propag.*, vol. 69, no. 11, pp. 7260-7268, Nov. 2021.

[14] J. Sun, Q. Cao, M. Pan and L. Zhu, "A Broadband Multilayer Absorber With Switchable Function of Radiation," *IEEE Trans. Antennas Propag.*, vol. 70, no. 8, pp. 6841-6849, Aug. 2022.

[15] Y. Han, L. Zhu, Y. Bo, W. Che and B. Li, "Novel Low-RCS Circularly Polarized Antenna Arrays via Frequency-Selective Absorber," *IEEE Trans. Antennas Propag.*, vol. 68, no. 1, pp. 287-296, Jan. 2020.

[16] H. Lin, Y. Li, S. -W. Wong, K. W. Tam, B. Liu and L. Zhu, "High-Selectivity FA-FA-Based Frequency Selective Surfaces Using Magnetoelectronic Dipole Antennas," *IEEE Trans. Antennas Propag.*, vol. 70, no. 11, pp. 10669-10677, Nov. 2022.

[17] L. Ge and K. M. Luk, "A Low-Profile Magneto-Electric Dipole Antenna," *IEEE Trans. Antennas Propag.*, vol. 60, no. 4, pp. 1684-1689, 2012.

[18] S. Zheng, Y. Yin, J. Fan, X. Yang, B. Li and W. Liu, "Analysis of Miniature Frequency Selective Surfaces Based on Fractal Antenna–Filter–Antenna Arrays," *IEEE Antennas Wireless Propag. Lett.*, vol. 11, pp. 240-243, 2012.

[19] M. S. Neiman, "The principle of reciprocity in antenna theory," *Proc. IRE*, vol. 31, no. 12, pp. 666–671, Dec. 1943.

[20] X. Q. Lin, P. Mei, P. C. Zhang, Z. Z. D. Chen and Y. Fan, "Development of a Resistor-Loaded Ultrawideband Absorber With Antenna Reciprocity," *IEEE Trans. Antennas Propag.*, vol. 64, no. 11, pp. 4910-4913, Nov. 2016.

[21] Z. Ma, C. Jiang, W. Cao, J. Li and X. Huang, "An Ultrawideband and High-Absorption Circuit-Analog Absorber With Incident Angle-Insensitive Performance," *IEEE Trans. Antennas Propag.*, vol. 70, no. 10, pp. 9376-9384, Oct. 2022.

[22] W. Yu, Y. Yu, W. Wang, X. H. Zhang and G. Q. Luo, "Low-RCS and Gain-Enhanced Antenna Using Absorptive/Transmissive Frequency Selective Structure," *IEEE Trans. Antennas Propag.*, vol. 69, no. 11, pp. 7912-7917, Nov. 2021.

[23] S. Ghosh and K. V. Srivastava, "An equivalent circuit model of FSS-based metamaterial absorber using coupled line theory," *IEEE Antennas Wireless Propag. Lett.*, vol. 14, pp. 511–514, 2015.

[24] W. Hofmann, C. Bornkessel, A. Schwind and M. A. Hein, "Challenges of RF Absorber Characterization: Comparison Between RCS- and NRL-Arch-Methods," *in 2019 Int. Symp. Electromagn. Compat.-EMC EUROPE)*, pp. 370-375, Sept. 2019.

[25] Wang, Ke, et al., "Broadband and broad-angle low-scattering metasurface based on hybrid optimization algorithm," Scientific Reports, vol. 4, no. 1, p. 5935, 2014.